Available on the CERN CDS information server **CMS PAS SUS-18-002**

CMS Physics Analysis Summary

Contact: cms-pag-conveners-susy@cern.ch 2018/09/17

Search for supersymmetry in events with a photon, jets, and missing transverse momentum in proton-proton collisions at 13 TeV

The CMS Collaboration

Abstract

A search for supersymmetry is presented based on events with at least one photon, multiple jets, and large missing transverse momentum produced in proton-proton collisions at a center-of-mass energy of $\sqrt{s} = 13$ TeV. The data correspond to an integrated luminosity of 35.9 fb^{-1} and were recorded by the CMS detector in 2016 at the LHC. The analysis characterizes signal-like events by categorizing the data into various signal regions based on the number of jets, the number of b-tagged jets, and missing transverse momentum. No significant excess of events is observed with respect to expectations from standard model processes. Limits are placed on gluino, top squark, and neutralino masses using several simplified models of pair production of supersymmetric particles with gauge-mediated supersymmetry breaking. Depending on the model and the mass of the next-to-lightest supersymmetric particle, gluino masses as large as 2120 GeV and top squark masses as large as 1230 GeV are excluded.

1 Introduction

The standard model (SM) of particle physics successfully describes many phenomena, but lacks several necessary elements to be a complete description of the universe, including a source for the relic abundance of dark matter (DM) [1, 2] in the universe. In addition, the SM must resort to fine-tuning [3–6] to explain the hierarchy between the Planck mass scale and the electroweak scale set by the vacuum expectation value of the Higgs field, the existence of which was recently confirmed by the observation of the Higgs boson [7, 8]. Supersymmetry (SUSY) [9–16] is an extension of the SM that can provide both a viable dark matter candidate and additional particles that naturally cancel large quantum corrections to the Higgs boson mass-squared term from the SM fields.

SUSY models predict a bosonic superpartner for each SM fermion and a fermionic superpartner for each SM boson; each new particle's spin differs from its SM partner by half a unit. SUSY also includes a second Higgs doublet. New colored states, like gluinos $\widetilde{\mathrm{g}}$ and top squarks $\widetilde{\mathrm{t}}$, the superpartners of the gluon and the top quark, respectively, are expected to have masses around 1 TeV in order to avoid fine-tuning in the SM Higgs boson mass-squared term. In R-parity [17] conserving models, each superpartner carries a conserved Z_2 quantum number that requires superpartners to be produced in pairs and causes the lightest supersymmetric particle (LSP) to be stable. The stable LSP can serve as a DM candidate.

The signatures targeted in this note are motivated by models in which gauge mediated symmetry breaking (GMSB) is responsible for separating the masses of the supersymmetric particles from their SM counterparts. In GMSB models, the gaugino masses are expected to be proportional to the size of their fundamental coupling. This includes the superpartner of the graviton, the gravitino, whose mass scales like $M_{\mathrm{SB}}/M_{\mathrm{Planck}}$, where M_{SB} represents the scale of the symmetry breaking interactions and M_{Planck} is the scale of gravity. GMSB permits a significantly lower symmetry breaking scale than, for example, gravity mediation, and therefore generically predicts that the gravitino will be the LSP [18–20], with a mass often much less than a GeV. Correspondingly, the next-to-lightest supersymmetric particle (NLSP) is typically a neutralino, a superposition of the superpartners of the neutral bosons. The details of the quantum numbers of the NLSP play a large part in determining the phenomenology of GMSB models, including final state mixtures of the Higgs boson, Z boson, and photon.

The scenario of a natural SUSY spectrum with GMSB and R-parity conservation typically manifests as events with multiple jets, at least one photon, and large $p_{\mathrm{T}}^{\mathrm{miss}}$, the magnitude of the missing transverse momentum. Depending on the topology, these jets can arise from either light- or heavy-flavored quarks. We study four simplified models [21–25], shown in Fig. 1. Three models involve gluino pair production, and one model involves top squark pair production. In the T5qqqqHG model, each gluino decays to a pair of light-flavored (u, d, s, c) quarks ($\mathrm{q\bar{q}}$) and a neutralino ($\widetilde{\chi}_1^0$). The T5bbbbZG and T5ttttZG models are similar to T5qqqqHG, except that the light-flavored quarks are replaced by a pair of bottom quarks ($\mathrm{b\bar{b}}$) and a pair of top quarks ($\mathrm{t\bar{t}}$), respectively. In the T5qqqqHG model, $\widetilde{\chi}_1^0$ decays either to a standard model Higgs boson and a gravitino ($\widetilde{\mathrm{G}}$) or to a photon and a gravitino. The $\widetilde{\chi}_1^0 \to \mathrm{H}\widetilde{\mathrm{G}}$ branching fraction is assumed to be 50%. In the T5bbbbZG and T5ttttZG models, the neutralinos decay to $\mathrm{Z}\widetilde{\mathrm{G}}$ and $\gamma\widetilde{\mathrm{G}}$ with equal probability. The T6ttZG model considers top squark pair production, with each top squark decaying into a top quark and a neutralino. The neutralino can then decay with equal probability to a photon and a gravitino or to a Z boson and a gravitino. In all models, the gravitino mass $m_{\widetilde{\mathrm{G}}}$ is fixed to be 1 GeV.

The data used in this search correspond to 35.9 fb^{-1} of proton-proton (pp) collisions and were

collected with the CMS detector during the 2016 run of the CERN LHC. The analysis selects signal regions distinguished by the number of jets N_{jets}, the number of tagged bottom quark jets $N_{\text{b-jets}}$, and large missing transverse momentum. The expected yields from SM backgrounds are estimated using a combination of simulations and data control regions. Comparisons between the expected background yields and the observed data yields are used to place limits on the gluino and top squark pair-production cross sections for the simplified models indicated above.

Previous searches for R-parity conserving SUSY with photons performed by the CMS Collaboration are documented in Refs. [26, 27]. This work improves on the previous results by including additional signal regions that exploit high jet and b-tagged jet multiplicities for sensitivity to high mass gluino models, and by increasing the usage of observed data for the background estimations. Similar searches have also been performed by the ATLAS Collaboration [28, 29].

A description of the CMS detector and the simulations used are presented in Section 2. The event reconstruction and signal region selections are presented in Section 3. The methods used for predicting the SM backgrounds are presented in Section 4. Results are given in Section 5. The analysis is summarized in Section 6.

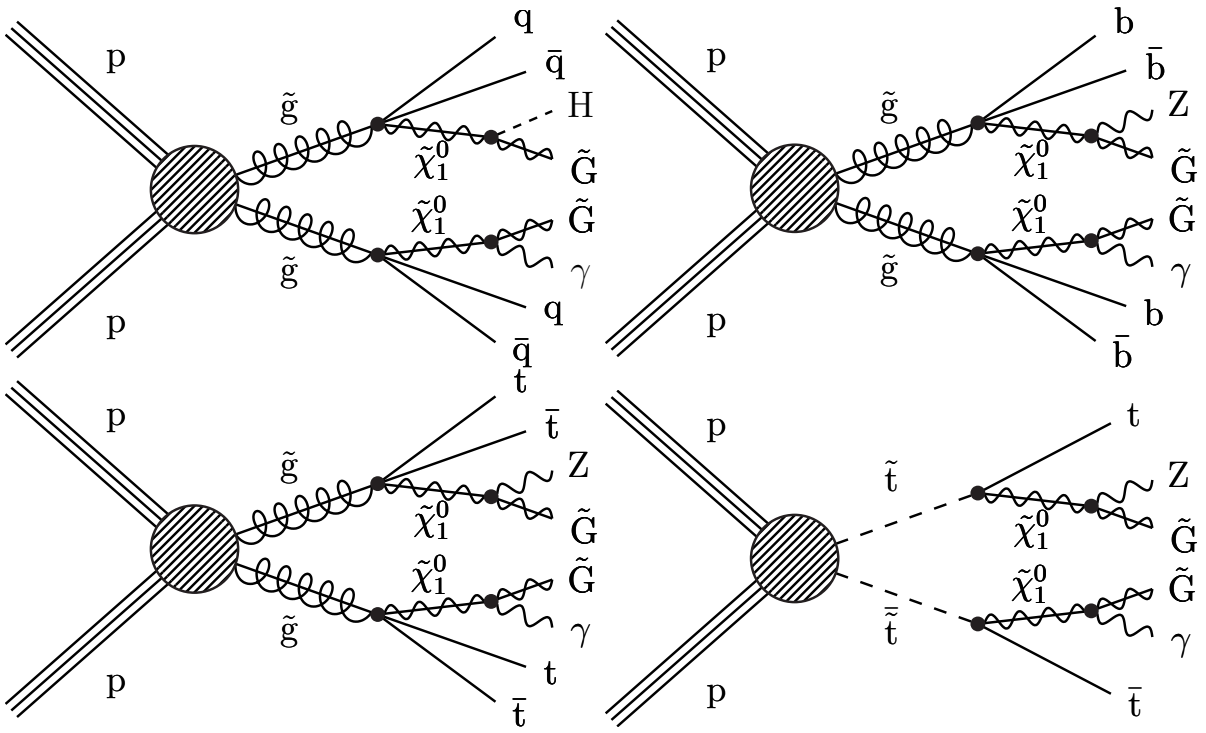

Figure 1: Example Feynman diagrams depicting the simplified models used. The top left diagram depicts the T5qqqqHG model, the top right diagram depicts the T5bbbbZG model, the bottom left diagram depicts the T5ttttZG model, and the bottom right depicts the T6ttZG model.

2 Detector and simulation

A detailed description of the CMS detector, along with a definition of the coordinate system and pertinent kinematic variables, is given in Ref. [30]. Briefly, a cylindrical superconducting solenoid with an inner diameter of 6 m provides a 3.8 T axial magnetic field. Within the cylindrical volume are a silicon pixel and strip tracker, a lead tungstate crystal electromagnetic calorimeter (ECAL), and a brass and scintillator hadron calorimeter (HCAL). The tracking de-

tectors cover the pseudorapidity range $|\eta| < 2.5$. The ECAL and HCAL, each composed of a barrel and two endcap sections, cover $|\eta| < 3.0$. Forward calorimeters extend the coverage to $3.0 < |\eta| < 5.0$. Muons are measured within $|\eta| < 2.4$ by gas-ionization detectors embedded in the steel flux-return yoke outside the solenoid. The detector is nearly hermetic, permitting accurate measurements of $p_{\mathrm{T}}^{\mathrm{miss}}$. The CMS trigger is described in Ref. [31].

Monte Carlo (MC) simulations are used to design the analysis, to facilitate background estimation methods using data control regions, and to predict event rates from simplified models. Simulated SM background processes include Vγ+jets (V = Z, W), $\mathrm{t\bar{t}}\gamma$, $\mathrm{t\bar{t}}$+jets, W+jets, and γ+jets. The SM background events are generated at leading order (LO) in perturbative quantum chromodynamics, except $\mathrm{t\bar{t}}\gamma$ which is generated at next-to-leading order (NLO), using the MADGRAPH5_aMC@NLO 2.2.2 or 2.3.3 generator [32] and the cross sections used for normalization are computed at NLO or next-to-NLO [32–43]. The diboson (Vγ), top quark, and vector boson plus jets events are generated with up to two, three, and four additional partons in the matrix element calculations, respectively.

The NNPDF3.0 [44] LO (NLO) parton distribution functions (PDFs) are used for samples simulated at LO (NLO). Parton showering and hadronization are described using the PYTHIA 8.212 generator [45] with the CUETP8M1 underlying event tune [46]. Partons generated with MADGRAPH5_aMC@NLO and PYTHIA that would otherwise be double counted are removed using the MLM [47] and FxFx [41] matching schemes in LO and NLO samples, respectively.

Signal samples are simulated at LO using the MADGRAPH5_aMC@NLO generator and their yields are normalized using NLO plus next-to-leading logarithmic (NLL) cross sections [48–52]. SUSY particles are modelled with PYTHIA.

The detector response to particles produced in the simulated collisions is modeled with the GEANT4 [53] detector simulation package for SM processes. Because of the large number of SUSY signals considered, with various gluino, squark, and neutralino masses, the detector response for these processes is simulated with the CMS fast simulation [54]. The results from the fast simulation generally agree with the results from the full simulation. Where there is disagreement, corrections are applied, most notably a correction of up to 14% to adjust for differences in the modeling of $p_{\mathrm{T}}^{\mathrm{miss}}$.

3 Event reconstruction and selection

The CMS particle-flow (PF) algorithm [55] is employed to reconstruct every particle in each event, using an optimal combination of information from all detector systems. Particle candidates are identified as charged hadrons, neutral hadrons, electrons, photons, or muons. For electron and photon PF candidates, further requirements are applied to the ECAL shower shape and the ratio of associated energies in the ECAL and HCAL [56, 57]. Similarly, for muon PF candidates, further requirements are applied to the matching between track segments in the silicon tracker and the muon detectors [58]. These further requirements improve the quality of the reconstruction. Electron and muon candidates are restricted to $|\eta| < 2.5$ and < 2.4, respectively. The missing transverse momentum $p_{\mathrm{T}}^{\mathrm{miss}}$ is calculated as the magnitude of the negative vector sum of the transverse momenta of all PF candidates.

After all interaction vertices are reconstructed, the primary pp interaction vertex is selected as the vertex with the largest sum of the squares of physics-object transverse momentum (p_{T}^2). The physics objects used in this calculation are produced by a jet finding algorithm [59, 60] applied to all charged-particle tracks associated to the vertex, plus the corresponding missing trans-

verse momentum computed from those jets. To mitigate the effect of secondary pp interactions (pileup), charged-particle tracks associated with vertices other than the primary vertex are not considered for jet clustering or calculating object isolation sums.

Jets are reconstructed by clustering PF candidates using the anti-k_T jet algorithm [59, 60] with a size parameter of 0.4. To eliminate spurious jets, for example those induced by electronics noise, further jet quality criteria [61] are applied. The jet energy response is corrected for the nonlinear response of the detector [62]. There is also a correction to account for the expected contributions of neutral particles from pileup, which cannot be removed based on association with secondary vertices [63]. Jets are required to have $p_T > 30\,\text{GeV}$ and are restricted to be within $|\eta| < 2.4$. The combined secondary vertex algorithm (CSVv2) at the medium working point [64] is applied to each jet to determine if it should be identified as a bottom quark jet. The CSVv2 algorithm at the specified working point has a 55% efficiency to correctly identify b jets with $p_T \approx 30\,\text{GeV}$. The corresponding misidentification probabilities are 1.6% for gluon and light-flavor quark jets, and 12% for charm quark jets.

Photons with $p_T > 100\,\text{GeV}$ and $|\eta| < 2.4$ are used in this analysis. To suppress jets erroneously identified as photons from neutral hadron decays, photon candidates are required to be isolated. An isolation cone specified by a radius $R = \sqrt{(\Delta\phi)^2 + (\Delta\eta)^2} < 0.2$ is used, with no dependence on the p_T of the photon candidate. Here, ϕ is the azimuthal angle. The energy measured in the isolation cone is corrected for contributions from pileup [63]. The shower shape and the fractions of hadronic and electromagnetic energy associated with the photon candidate are required to be consistent with expectations from prompt photons. The candidates matched to a track measured by the pixel detector (pixel seed) are rejected because they are likely to result from electrons that produced electromagnetic showers.

Similarly, to suppress jets erroneously identified as leptons and genuine leptons from hadron decays, electron and muon candidates are also subjected to isolation requirements. The isolation variable I is computed from the scalar p_T sum of selected charged hadron, neutral hadron, and photon PF candidates, divided by the lepton p_T. PF candidates enter the isolation sum if they satisfy $R < R_I$. The cone radius R_I decreases with lepton p_T because the collimation of the decay products of the parent particle of the lepton increases with the Lorentz boost of the parent [65]. The values used are $R_I = 0.2$ for $p_T^\ell < 50\,\text{GeV}$, $R_I = 10\,\text{GeV}/p_T^\ell$ for $50 \leq p_T^\ell \leq 200\,\text{GeV}$, and $Riso = 0.05$ for $p_T^\ell > 200\,\text{GeV}$, where $\ell = \text{e}, \mu$. As with photons, the expected contributions from pileup are subtracted from the isolation variable. The isolation requirement is $I < 0.1\ (0.2)$ for electrons (muons).

The electron, muon, and charged hadron PF candidates are also subjected to an isolation requirement, computed using tracks. The track isolation variable I_{track} is computed for each candidate from the scalar p_T sum of selected other charged-particle tracks, divided by the candidate p_T. Other charged-particle tracks are selected if they lie within a cone of radius 0.3 around the candidate direction. The isolation variable must satisfy $I_{\text{track}} < 0.2$ for electrons and muons, and $I_{\text{track}} < 0.1$ for charged hadrons. Isolated tracks are required to satisfy $|\eta| < 2.4$, and the transverse mass of each isolated track with p_T^{miss} is required to be less than 100 GeV.

Signal event candidates were recorded by requiring a photon at the trigger level with a transverse momentum requirement $p_T^\gamma > 90\,\text{GeV}$ if $H_T^\gamma = p_T^\gamma + \Sigma p_T^{\text{jet}} > 600\,\text{GeV}$ and $p_T^\gamma > 165\,\text{GeV}$ otherwise. The efficiency of this trigger, as measured in data, is 98% after applying the selection criteria described below. Additional triggers, requiring the presence of charged leptons, photons, or minimum $H_T = \Sigma p_T^{\text{jet}}$, are used to select samples employed in the evaluation of backgrounds.

Signal-like candidate events must fulfill one of two requirements, based on the trigger criteria described above: $p_{\mathrm{T}}^{\gamma} > 100\,\mathrm{GeV}$ and $H_{\mathrm{T}}^{\gamma} > 800\,\mathrm{GeV}$, or $p_{\mathrm{T}}^{\gamma} > 190\,\mathrm{GeV}$ and $H_{\mathrm{T}}^{\gamma} > 500\,\mathrm{GeV}$. In addition to these requirements, the events should have at least 2 jets and $p_{\mathrm{T}}^{\mathrm{miss}} > 100\,\mathrm{GeV}$. To reduce backgrounds from the SM processes that produce a leptonically decaying W boson, resulting in $p_{\mathrm{T}}^{\mathrm{miss}}$ from a neutrino, events are rejected if they have any charged light leptons (e, μ) with $p_{\mathrm{T}} > 10\,\mathrm{GeV}$ or any isolated electron, muon, or charged hadron tracks with $p_{\mathrm{T}} > 5, 5, 10\,\mathrm{GeV}$, respectively. Events from the γ+jets process typically satisfy the above criteria when the energy of a jet is mismeasured, inducing artificial $p_{\mathrm{T}}^{\mathrm{miss}}$. To reject these events, the two highest p_{T} jets are both required to have an angular separation from the $p_{\mathrm{T}}^{\mathrm{miss}}$ direction in the transverse plane, $\Delta\phi_{1,2} > 0.3$. Events with reconstruction failures, detector noise, or beam halo interactions are rejected using dedicated identification requirements [66].

The selected events are divided into 25 independent signal regions based on $p_{\mathrm{T}}^{\mathrm{miss}}$, the number of jets N_{jets}, and the number of b-tagged jets $N_{\text{b-jets}}$. The signal regions can be grouped into 6 categories based on N_{jets} and $N_{\text{b-jets}}$, whose intervals are defined to be N_{jets}: 2–4, 5–6, $\geq$7; and $N_{\text{b-jets}}$: 0, $\geq$1. Within each of the 6 categories, events are further distinguished based on 4 independent $p_{\mathrm{T}}^{\mathrm{miss}}$ regions, defined as: $200 < p_{\mathrm{T}}^{\mathrm{miss}} < 270, 270 < p_{\mathrm{T}}^{\mathrm{miss}} < 350, 350 < p_{\mathrm{T}}^{\mathrm{miss}} < 450$, and $p_{\mathrm{T}}^{\mathrm{miss}} > 450\,\mathrm{GeV}$. In the lowest N_{jets}, $N_{\text{b-jets}}$ category, the highest $p_{\mathrm{T}}^{\mathrm{miss}}$ bin is further subdivided into two intervals: $450 < p_{\mathrm{T}}^{\mathrm{miss}} < 750$ and $p_{\mathrm{T}}^{\mathrm{miss}} > 750\,\mathrm{GeV}$. Events with $100 < p_{\mathrm{T}}^{\mathrm{miss}} < 200\,\mathrm{GeV}$ are used as a control region for estimating SM backgrounds.

4 Background estimation

There are five main SM processes that can produce events mimicking our desired event signature of a photon, multiple jets, and $p_{\mathrm{T}}^{\mathrm{miss}}$. These processes are: W$\gamma$+jets and $\mathrm{t\bar{t}}\gamma$ with a high-p_{T} photon and a "lost" electron or muon (lost-lepton) or a hadronically decaying tau lepton (τ_{had}); $\mathrm{t\bar{t}}$+jets and W+jets, in which an electron from a W decay is erroneously identified as a photon; and Zγ+jets with a high-p_{T} photon, in which the Z boson decays to a pair of neutrinos. In all these events, the presence of one or more neutrinos is the source of genuine $p_{\mathrm{T}}^{\mathrm{miss}}$. The final category corresponds to the γ+jets process in which a mismeasured jet induces high $p_{\mathrm{T}}^{\mathrm{miss}}$. Quantum chromodynamics (QCD) multijet events with a jet misidentified as a photon and a highly mismeasured jet do not contribute significantly to the SM background.

The total event yield from each source of background is estimated separately for each of the 25 signal regions. The methods and uncertainties associated with the background predictions are detailed in the following sections.

4.1 Lost-lepton and τ_{had} backgrounds

The lost-lepton background arises from events in which the charged lepton from a leptonically decaying W boson cannot be identified. This can occur because the lepton is out of acceptance, fails the identification requirements, or fails the isolation requirements. For example, in events with high-p_{T} top quarks, the top quark decay products will be collimated, forcing the b jet to be closer to the charged lepton. In these cases, events are more likely to fail the isolation requirements. These events are estimated by studying control regions in both data and simulation, obtained by requiring both a well-identified photon and a light lepton (e, μ).

The τ_{had} background arises from events in which a W boson decays to a τ lepton, which subsequently decays to mesons and neutrinos. These hadronic decays of τ leptons occur $\approx$65% of the time. Because of lepton universality, the fraction of events with τ_{had} leptons can be estimated from the yield of events containing a single muon, after correcting for reconstruction

differences and for the τ_{had} branching fraction.

The lost-lepton and hadronic tau predictions rely on an extrapolation between eγ or $\mu\gamma$ event yields and single photon event yields. In all control regions where a single light lepton is required, the dominant SM processes that contribute are Wγ and t$\bar{\text{t}}\gamma$. Lost-muon and hadronic tau events are estimated using $\mu\gamma$ control regions, while lost-electron events are estimated using eγ control regions. In each control region, exactly one electron or muon is required and the isolated track veto for the selected lepton flavor is ignored. In order to reduce the effect of signal contamination, events are only selected if the transverse mass of the lepton-$p_{\text{T}}^{\text{miss}}$ system, $m_{\text{T}} = \sqrt{2p_{\text{T}}^{\ell}p_{\text{T}}^{\text{miss}}(1-\cos\Delta\phi)}$, is less than 100 GeV. All other kinematic variable requirements for each signal region are applied to the corresponding control regions.

An average transfer factor is derived using simulations of the Wγ+jets and t$\bar{\text{t}}\gamma$ processes, which determine the number of events expected in the signal region for each eγ or $\mu\gamma$ event observed in the control region. The transfer factors applied to the $\mu\gamma$ control regions account for both lost-μ events and τ_{had} events, and are typically in the range $0.7 < T_{\mu,\tau} < 1.0$. The transfer factors applied to eγ events account for only the lost-e events and are typically in the range $0.3 < T_{\text{e}} < 0.6$. The transfer factors are parameterized versus N_{jets}, $N_{\text{b-jets}}$, and $p_{\text{T}}^{\text{miss}}$; however, for $p_{\text{T}}^{\text{miss}} > 150$ GeV, T_{ℓ} is found to be independent of $p_{\text{T}}^{\text{miss}}$. The parameterization of the transfer factors is validated using simulation by treating eγ or $\mu\gamma$ events like data and comparing the predicted lost-lepton and τ_{had} event yields to the true simulated event yields in the signal regions. This validation is shown in Fig. 2. The prediction in each signal region is $N_{\ell}^{\text{pred}} = \Sigma_i N_i T_{\ell,i}$, where $\ell = \text{e}, \mu$ and i ranges from 1 to n, where n is the number of transfer factors that contribute in a given signal region.

The dominant uncertainty in the lost-lepton predictions arises from the limited numbers of events in the eγ and $\mu\gamma$ control regions. These uncertainties are modeled in our final statistical interpretations as a gamma distribution whose shape parameter is set by the observed number of events and whose scale parameter is the average transfer factor for that bin. Other systematic uncertainties in the determination of the transfer factors include jet energy correction uncertainties, parton distribution function uncertainties, renormalization (μ_R) and factorization (μ_F) scale uncertainties, and simulation correction factor uncertainties. The uncertainties in μ_R and μ_F are obtained by varying these values independently by factors of 0.5 and 2.0 [67, 68]. Simulation correction factors are used to account for differences between the observed data and modeling of b-tagging efficiencies in simulation, b jet misidentification, and lepton reconstruction efficiencies.

4.2 Misidentified photon background

Events containing the decay $\text{W} \to \text{e}\nu_{\text{e}}$ are the primary source of electrons that are erroneously identified as photons. Photon misidentification can occur when a pixel seed fails to be associated with the candidate object. Given a misidentification rate, which relates events with a well-identified electron to events with an erroneously identified photon, the photon background can be estimated from a single electron (zero photons) control region. The misidentification rate is estimated in simulation and corrections are derived from observed data to account for any mismodeling in simulation.

The single electron control regions are defined by the same kinematic requirements as the single photon signal regions, except that we require exactly zero photons and exactly one electron, and we use the momentum of the electron in place of the momentum of the photon for photon-based variables. In addition to all of the signal region selections, events are also required to

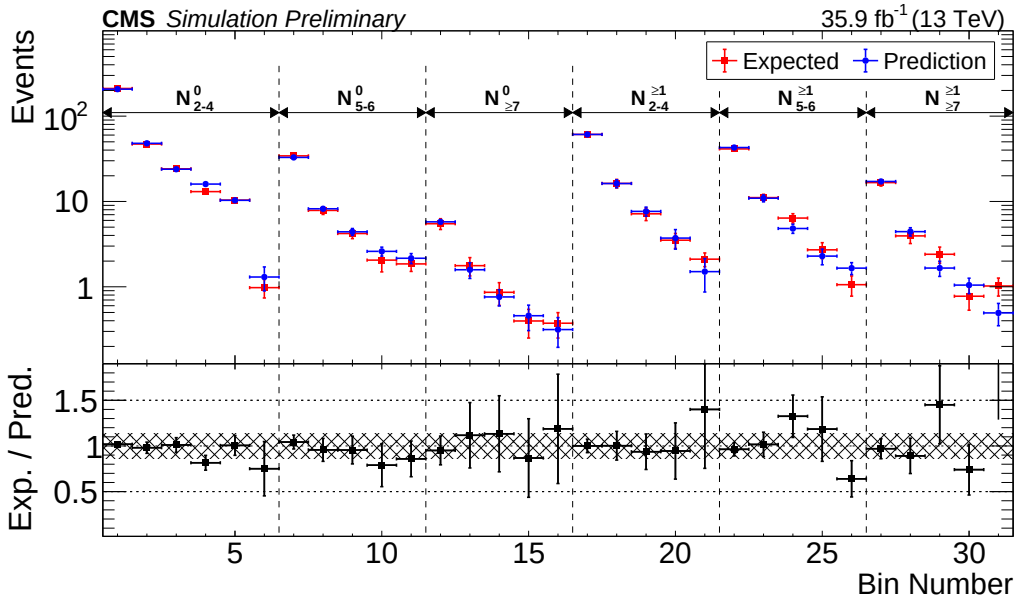

Figure 2: The lost-lepton and τ_{had} event yields as predicted directly from simulation in the signal regions, shown in red, and from the prediction procedure applied to simulated eγ or $\mu\gamma$ events, shown in blue. The error bars correspond to the statistical uncertainties from the limited number of events in simulation. The bottom panel shows the ratio of the simulation expectation (Exp.) and the simulation-based prediction (Pred.). The hashed area shows the expected uncertainties from parton distribution functions, renormalization and factorization scale uncertainties, and data-to-simulation correction factor uncertainties. The categories, denoted by dashed lines, are labeled as N_j^b, where j refers to the number of jets and b refers to the number of b-tagged jets. The numbered bins within each category are the various p_T^{miss} bins. In each of these regions, the first bin corresponds to $100 < p_T^{\text{miss}} < 200\,\text{GeV}$, which is used for SM predictions. Note that the kinematic variable requirements used to derive the average transfer factors are different from those used to define the search regions. Expectations and predictions are compatible within uncertainties.

satisfy $m_T(e, p_T^{\text{miss}}) < 100\,\text{GeV}$.

To extrapolate from the event yields in the single electron control regions to the event yields for the misidentified photon background in the signal regions, we derive a misidentification rate $f = N_\gamma/N_e$ using a combination of simulation and data. The misidentification rate is determined as a function of the electron p_T and the multiplicity Q_{mult} of charged-particle tracks in a region around the electron candidate. The charged track multiplicity is computed by counting the number of charged PF candidates (electrons, muons, hadrons) in the jet closest to the electron candidate. If there is no jet within $\Delta R = \sqrt{\Delta\phi^2 + \Delta\eta^2} < 0.3$ of the electron candidate, Q_{mult} is defined to be zero. A typical event in the single electron control region has a Q_{mult} of 3–4. The p_T^{miss} and Q_{mult} dependence of the misidentification rate is derived using simulated W+jets and $\bar{\text{t}}\text{t}$+jets events. The misidentification rate is on average 1–2%, but can be as low as 0.5% for events with high Q_{mult}.

To account for systematic differences between the simulation and data misidentification rates, we correct the misidentification rate by measuring it in both simulated and observed Drell–Yan (DY) events. Separate corrections are derived for low Q_{mult} ($\leq$1) and high Q_{mult} ($\geq$2). The DY control region is defined by requiring one electron with $p_T > 40\,\text{GeV}$ and another reconstructed particle, either a photon or an oppositely-charged electron, with $p_T > 100\,\text{GeV}$. A further

requirement $50 < m_{e^+e^-}, m_{e\gamma} < 130\,\text{GeV}$ is applied to ensure the particles are consistent with the decay products of a Z boson, and therefore the photon is likely to be a misidentified electron. The misidentification rate is computed as the ratio $N_{e\gamma}/N_{e^+e^-}$, where N_{ij} is the number of events in the control region containing particles i and j. It is found to be 15–20% higher in the data than in the simulation.

The prediction of misidentified photons in the signal region is then given by the weighted sum of the observed events in the control region, where the weight is given by the data-corrected misidentification rate for photons. Uncertainties on these predictions are dominated by the data-to-simulation corrections and the limited number of events in the simulation at large values of p_T^{miss}. The misidentified photon background prediction also includes uncertainties in the modeling of initial-state radiation (ISR) in the simulation, statistical uncertainties from the limited number of events in the data control regions, uncertainties from pileup modeling, and uncertainties in the trigger efficiency measurement.

4.3 Background from $Z(\nu\bar{\nu})\gamma$ events

Decays of the Z boson to invisible particles constitute a major background for events with low N_{jets}, low $N_{b\text{-jets}}$, and high p_T^{miss}. The $Z(\nu\bar{\nu})\gamma$ background is estimated using $Z(\ell^+\ell^-)\gamma$ events. The shape of the distribution of p_T^{miss} vs. N_{jets} in $Z(\nu\bar{\nu})\gamma$ events is modeled with the simulation, while the normalization and the purity of the control region are measured in data.

Events in the $\ell^+\ell^-\gamma$ control region are required to have exactly two oppositely-charged, same-flavor leptons (ℓ = e or μ) and one photon with $p_T > 100\,\text{GeV}$. The dilepton invariant mass $m_{\ell\ell}$ is required to be consistent with the Z boson mass, $80 < m_{\ell\ell} < 100\,\text{GeV}$. The charged leptons serve as a proxy for neutrinos, so the event-level kinematic variables, such as p_T^{miss}, are calculated after removing charged leptons from the event.

The $\ell^+\ell^-\gamma$ control region may contain a small proportion of events from processes other than $Z(\ell^+\ell^-)\gamma$, primarily $t\bar{t}\gamma$. We define the purity of the control region as the percentage of events originating from the $Z(\ell^+\ell^-)\gamma$ process. The purity is computed in data by measuring the number of events in the corresponding oppositely-charged, opposite-flavor control region, which has a higher proportion of $t\bar{t}\gamma$ events. The purity is found to be $(97 \pm 3)\%$. A statistically compatible purity is also measured in the oppositely-charged, same-flavor control region. In this region, the $m_{\ell\ell}$ distribution is used to extrapolate from the number of events with $m_{\ell\ell}$ far from the Z boson mass to the number of events with $m_{\ell\ell}$ close to the Z boson mass.

The $Z(\nu\bar{\nu})\gamma$ predictions from simulation are scaled to the total $Z(\ell^+\ell^-)\gamma$ yield observed according to $N_{Z(\nu\bar{\nu})\gamma} = \beta R_{\nu\nu/\ell\ell} N_{Z(\ell^+\ell^-)\gamma}$, where β is the purity of the $Z(\ell^+\ell^-)\gamma$ control region and $R_{\nu\nu/\ell\ell}$ is the ratio between the expected number of $Z(\nu\bar{\nu})\gamma$ and $Z(\ell^+\ell^-)\gamma$ events. The ratio $R_{\nu\nu/\ell\ell}$, which accounts for lepton reconstruction effects and the relative branching fractions for $Z \to \nu\bar{\nu}$ and $Z \to \ell^+\ell^-$, is computed from the simulation.

The primary uncertainty in the $Z(\nu\bar{\nu})\gamma$ prediction arises from uncertainties in the p_T^{miss} distribution from the simulation. Other uncertainties include statistical uncertainties from the limited number of events in the simulation and uncertainties in the estimation of the control region purity. The p_T^γ-dependent NLO electroweak corrections [69] are assigned as additional uncertainties to account for any mismodeling of the photon p_T in the simulation. This uncertainty has a magnitude of 8% for the lowest p_T^{miss} bin and rises to 40% for $p_T^{miss} > 750\,\text{GeV}$.

4.4 Background from γ+jets events

The γ+jets background is dominated by events in which the p_T of an energetic jet is mismeasured, resulting in high p_T^{miss}. The QCD multijet events with a jet misidentified as a photon and a mismeasured jet contribute to this background at a much smaller rate; these events are measured together with events from the γ+jets process. Most of these events are removed by requiring that the azimuthal angles between the p_T^{miss} and each of the two highest p_T jets satisfy $\Delta\phi_{1,2} > 0.3$. Inverting this requirement provides a large control region of low-$\Delta\phi$ events that is used to predict the γ+jets background in the signal regions. The ratio of high-$\Delta\phi$ events to low-$\Delta\phi$ events, $R_{h/l}$, is derived from the low-p_T^{miss} sideband ($100 < p_T^{miss} < 200\,GeV$).

While most of the events in both the low-$\Delta\phi$ and the low-p_T^{miss} control regions are γ+jets events, electroweak backgrounds in which p_T^{miss} arises from W or Z bosons decaying to one or more neutrinos, like those discussed previously, will contaminate these control regions. This can be significant for high N_{jets} and $N_{b\text{-}jets}$, where $t\bar{t}$ events are more prevalent. The rates of these events in the control regions are predicted using the same techniques discussed in the previous sections.

Because $R_{h/l}$ depends on p_T^{miss}, a double ratio $\kappa = R_{h/l}^{p_T^{miss}<200} / R_{h/l}^{p_T^{miss}>200}$ is derived from simulated γ+jets events in order to account for this correlation. To test how well the simulation models κ, we use a zero photon validation region in which the contribution from events containing a mismeasured jet dominates. To be consistent with the trigger used to select the data in this region, these events are also required to have $H_T > 1000\,GeV$. Electroweak contamination in the zero photon validation region is estimated using Vγ+jets (V = Z, W), $t\bar{t}\gamma$, $t\bar{t}$+jets, W+jets, QCD multijets, and $Z(\nu\bar{\nu})$+jets simulated events. The comparison of κ in data and simulation is shown in Fig. 3. The level of disagreement is found to be less than 20%.

Event yields for the γ+jets background are computed from the high-p_T^{miss}, low-$\Delta\phi$ control regions according to $N_{\gamma+jets} = \kappa N_{low\text{-}\Delta\phi} R_{h/l}$. $N_{low\text{-}\Delta\phi}$ is the event yield in the high-p_T^{miss}, low-$\Delta\phi$ control region after removing contributions from electroweak backgrounds.

Uncertainties in the γ+jets prediction are dominated by statistical uncertainties either from the limited number of events in the low-$\Delta\phi$ control regions or from the predictions of the electroweak contamination. The <20% disagreement between the κ values in data and simulation in the zero photon validation region is included as an additional uncertainty. Uncertainties in b-tagging correction factors are a minor contribution to the uncertainty in the γ+jets prediction.

5 Results

The predicted background and observed yields are shown in Table 1 and Fig. 4. The largest deviation is found in bin 2 ($2 \leq N_{jets} \leq 4$, $N_{b\text{-}jets} = 0$, and $270 < p_T^{miss} < 350\,GeV$), where the background is predicted to be 91 events with 51 events observed, corresponding to 4.3 standard deviations below the SM expectation. As described below, the results are interpreted after constraining background predictions and uncertainties to observation through a maximum likelihood fit that assumes no signal. Because of nonnegligible uncertainties in the background prediction in bin 2, these adjustments have the effect of reducing the observed discrepancy in bin 2 to approximately two standard deviations. In general, a large deviation in a single bin is inconsistent with the expectations from the signal models considered here. The observations in all other bins are consistent with SM expectations within one standard deviation.

Limits are evaluated for the production cross sections of the signal scenarios discussed in Section 1 using a maximum likelihood fit for the SUSY signal strength, the yields of the five classes

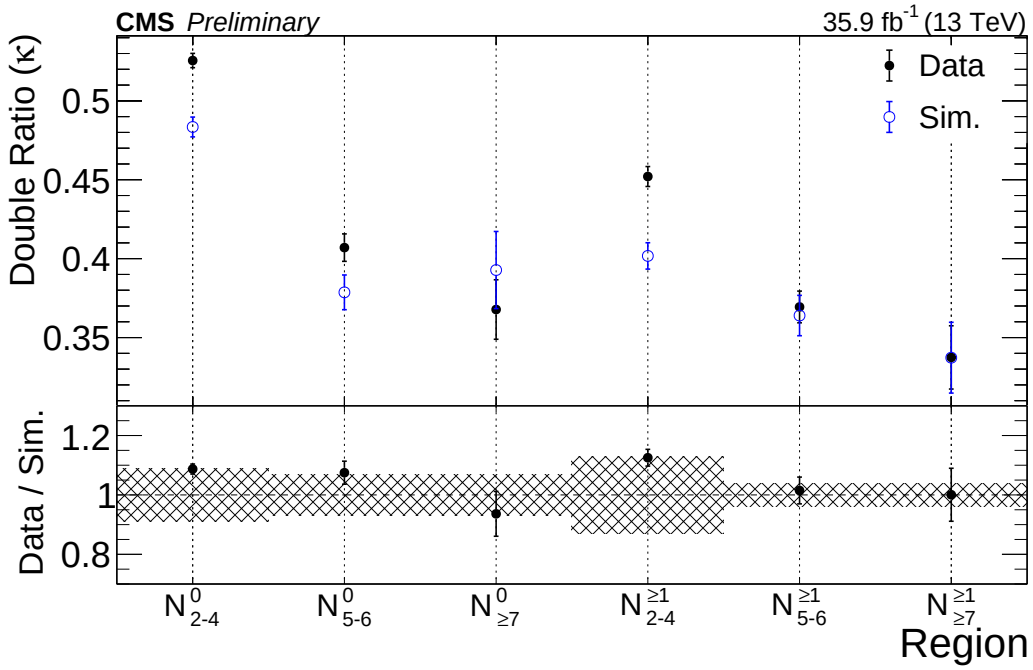

Figure 3: Validation of the double ratio κ in each N_{jets}-$N_{\text{b-jets}}$ region for zero photon events. The black points are the observed κ values after subtracting the electroweak contamination based on the simulation. The blue points are the κ values computed directly from the simulation. The ratio is shown in the bottom panel, where the hashed region corresponds to the systematic uncertainty in the γ+jets prediction. In the label N_{j}^{b}, j refers to the number of jets and b refers to the number of b-tagged jets.

of background events shown in Fig. 4, and various nuisance parameters. A nuisance parameter refers to a variable of little physical interest, such as the effect of parton distribution function uncertainties in a background prediction. The nuisance parameters are constrained by observed data in the fit. The uncertainties in the predicted signal yield arise from uncertainties in renormalization and factorization scales, ISR modeling, jet energy scale, b-tagging efficiency and misidentification, corrections to simulation, and limited numbers of simulated events. The largest uncertainty comes from the ISR modeling; it ranges from 3–4% depending on the signal region and the signal parameters, taking higher values for regions with large N_{jets} or for signals with $\Delta m \approx 0$. Here, Δm is the difference in mass between a gluino or squark and its decay products, e.g. $\Delta m = m_{\tilde{\text{g}}} - (m_{\tilde{\chi}_1^0} + 2m_{\text{t}})$ for the T5ttttZG model when on-shell top quarks are produced. The second largest uncertainty comes from the correction for differences between GEANT4 and the fast simulation in $p_{\text{T}}^{\text{miss}}$ modeling, with a maximum value of 10%. More details on the sources of systematic uncertainty in the signal predictions can be found in Ref. [70].

For the models of gluino pair production considered here, the limits are derived as a function of $m_{\tilde{\text{g}}}$ and $m_{\tilde{\chi}_1^0}$, while for the model of top squark pair production, the limits are a function of $m_{\tilde{\text{t}}}$ and $m_{\tilde{\chi}_1^0}$. The likelihood used for the statistical interpretation models each of the signal regions as a Poisson distribution, multiplied by constraints which account for uncertainties in the background predictions and signal yields. For predictions in which an observed event yield in a control region is scaled, a gamma distribution is used to model the Poisson uncertainty of the observed control region yield. All other uncertainties are modeled as log-normal distributions. The test statistic is $q_\mu = -2\ln \mathcal{L}_\mu / \mathcal{L}_{\text{max}}$, where $\mathcal{L}_{\text{max}}$ is the maximum likelihood determined by allowing all parameters, including the signal strength, to float, and $\mathcal{L}_\mu$ is the maximum likeli-

hood for a fixed value of μ. Limits are determined using an approximation of the asymptotic form of the test statistic distribution [71] in conjunction with the CL_s criterion [72, 73]. Expected upper limits are derived by varying observed yields according to expectations from the background-only hypothesis.

Using the statistical procedure described above, 95% confidence level (CL) upper limits are computed on the signal cross section for each simplified model and each mass point. Exclusion limits are defined by comparing observed upper limits to the predicted NLO+NLL signal cross section. The signal cross sections are also varied according to theory uncertainties to give a $\pm 1\sigma$ variation on the observed exclusion contour. The 95% CL limits and exclusion contours for the four models considered, T5qqqqHG, T5bbbbZG, T5ttttZG, and T6ttZG, are shown in Fig. 5.

Generally, the limits degrade at both high and low $m_{\widetilde{\chi}_1^0}$. For $m_{\widetilde{\chi}_1^0} \approx m_{\widetilde{g}}\,(m_{\widetilde{t}})$, the quarks from the decay of gluinos (top squarks) have low p_T. Correspondingly, the H_T^γ, N_{jets}, and $N_{\text{b-jets}}$ distributions tend toward lower values, reducing the signal efficiency and causing signal events to populate regions with higher background yields. Model points with small $m_{\widetilde{\chi}_1^0}$ have high momentum quarks produced in the decay of gluinos or top squarks, but have lower p_T^{miss} on average. For all models except T5qqqqHG, when the NLSP mass drops below the mass of the Z boson, the kinematics of the NLSP decay require the Z boson to be far from its pole mass. Therefore, the LSP carries a larger fraction of the momentum of the NLSP and thus produces larger p_T^{miss}. This increase in p_T^{miss} at low $m_{\widetilde{\chi}_1^0}$ is the cause of the increase in sensitivity in this region of parameter space. While a similar effect would happen for the T5qqqqHG model, the set of simulations used here does not probe the region of parameter space where the Higgs boson would be forced to have a mass far from its pole mass.

For moderate $m_{\widetilde{\chi}_1^0}$, the observed (expected) exclusion limits are as large as 2090 GeV (2100 GeV) for the T5qqqqHG model, 2120 GeV (2140 GeV) for T5bbbbZG, 1970 GeV (2000 GeV) for T5ttttZG, and 1230 GeV (1240 GeV) for T6ttZG. For small $m_{\widetilde{\chi}_1^0}$, the expected (observed) exclusion limits are at least 1920 GeV (1910 GeV) for the T5qqqqHG model, 1950 GeV (1960 GeV) for T5bbbbZG, 1800 GeV (1800 GeV) for T5ttttZG, and 1110 GeV (1110 GeV) for T6ttZG.

6 Summary

A search for gluino and top squark pair production is presented, based on proton-proton collisions dataset with a center-of-mass energy of 13 TeV recorded in 2016 with the CMS detector. The data correspond to an integrated luminosity of $35.9\,\text{fb}^{-1}$. Events are required to have at least one isolated photon with $p_T > 100\,\text{GeV}$, two jets with $p_T > 30\,\text{GeV}$ and $|\eta| < 2.4$, and large missing transverse momentum $p_T^{\text{miss}} > 200\,\text{GeV}$.

The data are categorized into 25 independent signal regions based on the number of jets, the number of b-tagged jets, and p_T^{miss}. Background yields from standard model processes are predicted using simulation and data control regions. The observed event yields are found to be consistent with expectations from the SM processes within uncertainties.

Results are interpreted in the context of simplified models. Four such models are studied, three of which involve gluino pair production and one of which involves top squark pair production. All models assume a gauge-mediated supersymmetry breaking scenario, in which the lightest supersymmetric particle is a gravitino. We consider scenarios in which the gluino decays to a neutralino $\widetilde{\chi}_1^0$ and a pair of light-flavor quarks (T5qqqqHG), bottom quarks (T5bbbbZG), or top quarks (T5ttttZG). In the T5qqqqHG model, the $\widetilde{\chi}_1^0$ decays either to a photon and gravitino $\widetilde{G}$ or

Table 1: Predicted and observed event yields for each signal region.

N_{jets}	$N_{\text{b-jets}}$	$p_{\text{T}}^{\text{miss}}$ [GeV]	Lost e	Lost μ+ τ_{had}	Misid. γ	$Z(\nu\bar{\nu})\gamma$	γ+jets	Total	Data
2–4	0	200–270	10.5 ± 2.6	31.2 ± 6.0	22.3 ± 5.4	33.6 ± 8.3	60 ± 11	157 ± 16	151
2–4	0	270–350	5.8 ± 1.8	29.6 ± 5.9	11.9 ± 2.9	22.9 ± 6.0	20.5 ± 4.3	91 ± 10	51
2–4	0	350–450	1.68 ± 0.88	13.9 ± 3.9	6.6 ± 1.6	17.0 ± 5.2	4.1 ± 1.4	43.3 ± 6.8	50
2–4	0	450–750	1.98 ± 0.94	8.1 ± 3.1	6.7 ± 1.5	18.1 ± 7.1	2.5 ± 1.3	37.4 ± 8.0	33
2–4	0	>750	$0.00^{+0.69}_{-0.00}$	1.2 ± 1.2	0.79 ± 0.19	2.8 ± 1.2	$0.41^{+0.42}_{-0.41}$	5.2 ± 1.9	6
5–6	0	200–270	1.28 ± 0.61	5.1 ± 1.9	3.53 ± 0.75	3.09 ± 0.78	15.8 ± 4.8	28.8 ± 5.3	26
5–6	0	270–350	2.06 ± 0.80	3.2 ± 1.5	2.39 ± 0.56	1.98 ± 0.54	3.7 ± 1.8	13.3 ± 2.6	11
5–6	0	350–450	0.77 ± 0.46	$0.64^{+0.65}_{-0.64}$	1.26 ± 0.30	1.49 ± 0.47	1.23 ± 0.97	5.4 ± 1.4	8
5–6	0	>450	0.26 ± 0.26	1.9 ± 1.1	1.00 ± 0.24	1.65 ± 0.65	$0.07^{+0.52}_{-0.07}$	4.9 ± 1.4	7
$\geq$7	0	200–270	$0.00^{+0.61}_{-0.00}$	$0.0^{+1.3}_{-0.0}$	0.72 ± 0.16	0.37 ± 0.11	1.8 ± 1.2	2.9 ± 1.9	3
$\geq$7	0	270–350	$0.34^{+0.35}_{-0.34}$	1.5 ± 1.0	0.38 ± 0.10	0.24 ± 0.08	1.22 ± 0.94	3.6 ± 1.5	3
$\geq$7	0	350–450	$0.34^{+0.35}_{-0.34}$	0.73 ± 0.73	0.17 ± 0.05	0.16 ± 0.07	$0.07^{+0.50}_{-0.07}$	1.46 ± 0.96	0
$\geq$7	0	>450	$0.00^{+0.61}_{-0.00}$	$0.0^{+1.3}_{-0.0}$	0.20 ± 0.06	0.17 ± 0.08	$0.00^{+0.75}_{-0.00}$	$0.37^{+1.60}_{-0.37}$	0
2–4	$\geq$1	200–270	3.4 ± 1.5	14.5 ± 4.2	7.1 ± 1.7	3.55 ± 0.89	11.3 ± 3.3	39.8 ± 5.9	50
2–4	$\geq$1	270–350	2.9 ± 1.4	5.6 ± 2.5	3.79 ± 0.92	2.45 ± 0.65	5.7 ± 1.8	20.4 ± 3.6	20
2–4	$\geq$1	350–450	$0.0^{+1.0}_{-0.0}$	1.1 ± 1.1	2.00 ± 0.45	1.81 ± 0.55	0.59 ± 0.44	5.5 ± 1.7	4
2–4	$\geq$1	>450	2.3 ± 1.2	4.4 ± 2.3	1.62 ± 0.38	2.14 ± 0.84	0.95 ± 0.54	11.5 ± 2.8	8
5–6	$\geq$1	200–270	3.5 ± 1.3	2.4 ± 1.4	5.5 ± 1.2	0.76 ± 0.20	7.7 ± 2.4	19.9 ± 3.3	21
5–6	$\geq$1	270–350	1.06 ± 0.64	4.0 ± 1.8	2.98 ± 0.63	0.49 ± 0.14	2.1 ± 1.0	10.6 ± 2.3	15
5–6	$\geq$1	350–450	0.71 ± 0.51	2.4 ± 1.4	1.38 ± 0.29	0.32 ± 0.11	$0.30^{+0.49}_{-0.30}$	5.1 ± 1.6	6
5–6	$\geq$1	>450	$0.35^{+0.36}_{-0.35}$	$0.0^{+1.4}_{-0.0}$	0.67 ± 0.15	0.48 ± 0.20	$0.00^{+0.56}_{-0.00}$	$1.5^{+1.6}_{-1.5}$	2
$\geq$7	$\geq$1	200–270	0.72 ± 0.53	2.0 ± 1.2	1.68 ± 0.37	0.13 ± 0.04	5.9 ± 5.0	10.5 ± 5.1	12
$\geq$7	$\geq$1	270–350	$0.00^{+0.65}_{-0.00}$	1.33 ± 0.96	0.73 ± 0.16	0.10 ± 0.04	$0.0^{+1.1}_{-0.0}$	2.2 ± 1.6	1
$\geq$7	$\geq$1	350–450	0.72 ± 0.53	$0.0^{+1.2}_{-0.0}$	0.44 ± 0.10	0.07 ± 0.03	$0.0^{+1.1}_{-0.0}$	$1.2^{+1.7}_{-1.2}$	1
$\geq$7	$\geq$1	>450	$0.36^{+0.37}_{-0.36}$	$0.0^{+1.2}_{-0.0}$	0.23 ± 0.07	0.04 ± 0.02	$0.0^{+1.1}_{-0.0}$	$0.6^{+1.7}_{-0.6}$	1

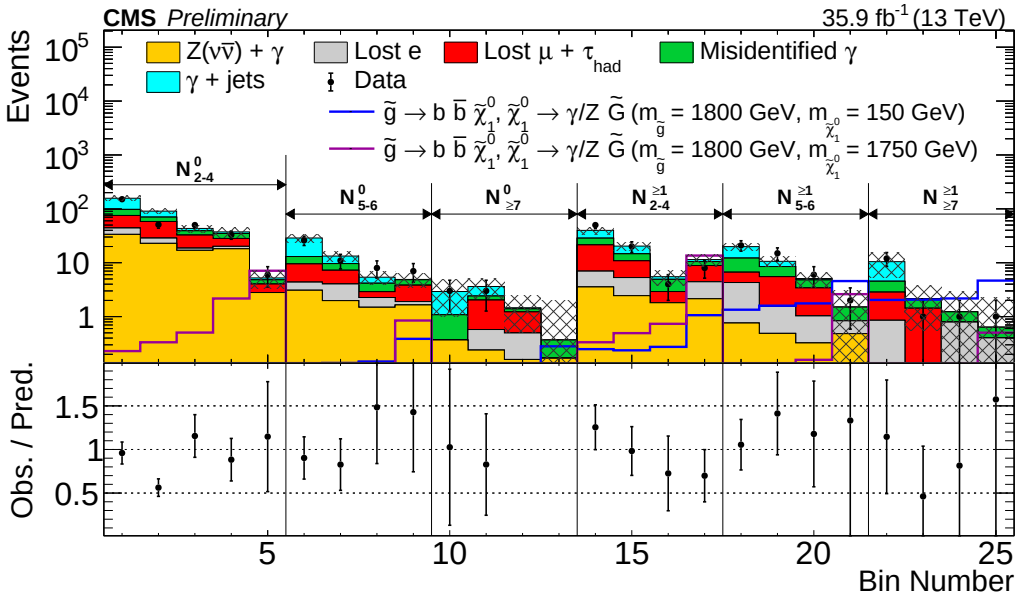

Figure 4: Distribution of predicted SM background events from various sources and observed events in each of the 25 signal regions. The categories, denoted by dashed lines, are labeled as N_j^b, where j refers to the number of jets and b refers to the number of b-tagged jets. The numbered bins within each category are the various p_T^{miss} bins. The lower pane shows the ratio of observed events to predicted SM background events. The error bars in the lower pane are the quadrature sum of the statistical uncertainty in the observed data and the systematic uncertainty in the predicted backgrounds before adjustments based on a maximum likelihood fit to data assuming a signal strength of zero. The observed event yields are consistent with the predicted SM backgrounds within one standard deviation in all bins except bin 2, as discussed in the text.

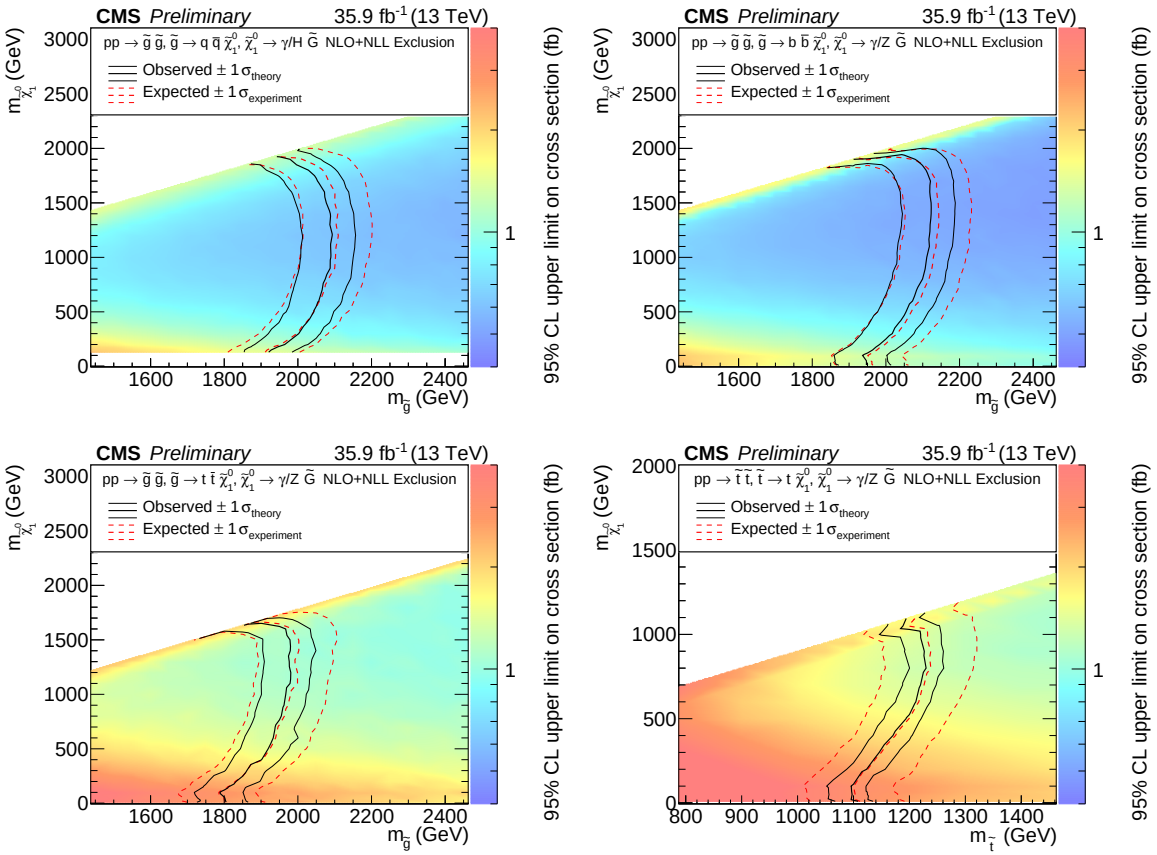

Figure 5: Observed and expected 95% CL upper limits for gluino or top squark pair production cross sections for the (upper left) T5qqqqHG, (upper right) T5bbbbZG, (bottom left) T5ttttZG, and (bottom right) T6ttZG models. Black lines denote the observed exclusion limit and the uncertainty due to variations of the theoretical prediction of the gluino or top squark pair production cross section. The dashed lines correspond to the region containing 68% of the distribution of the expected exclusion limits under the background-only hypothesis.

to a Higgs boson and $\widetilde{\mathrm{G}}$, with branching fraction 50%. In the T5bbbbZG and T5ttttZG models, the $\widetilde{\chi}_1^0$ decays either to a photon and $\widetilde{\mathrm{G}}$ or to a Z boson and $\widetilde{\mathrm{G}}$, with branching fraction 50%. In the top squark pair production model (T6ttZG), top squarks decay to a top quark and $\widetilde{\chi}_1^0$, and the $\widetilde{\chi}_1^0$ decays to a photon and $\widetilde{\mathrm{G}}$ or to a Z boson and $\widetilde{\mathrm{G}}$ with a branching fraction of 50%.

Using the next-to-leading-order plus next-to-leading-logarithmic cross sections for supersymmetric pair production, we place 95% confidence level upper limits on the gluino mass as large as 2120 GeV, depending on the model and $m_{\widetilde{\chi}_1^0}$, and limits on the top squark mass as large as 1230 GeV, depending on $m_{\widetilde{\chi}_1^0}$. These results improve upon those from previous searches for supersymmetry with photons [26, 27].

References

[1] F. Zwicky, "Die rotverschiebung von extragalaktischen nebeln", *Helv. Phys. Acta* **6** (1933) 110.

[2] V. C. Rubin and W. K. Ford Jr, "Rotation of the Andromeda nebula from a spectroscopic survey of emission regions", *Astrophys. J.* **159** (1970) 379, doi:10.1086/150317.

[3] R. Barbieri and G. F. Giudice, "Upper bounds on supersymmetric particle masses", *Nucl. Phys. B* **306** (1988) 63, doi:10.1016/0550-3213(88)90171-X.

[4] S. Dimopoulos and G. F. Giudice, "Naturalness constraints in supersymmetric theories with nonuniversal soft terms", *Phys. Lett. B* **357** (1995) 573, doi:10.1016/0370-2693(95)00961-J, arXiv:hep-ph/9507282.

[5] R. Barbieri and D. Pappadopulo, "S-particles at their naturalness limits", *JHEP* **10** (2009) 061, doi:10.1088/1126-6708/2009/10/061, arXiv:0906.4546.

[6] M. Papucci, J. T. Ruderman, and A. Weiler, "Natural SUSY endures", *JHEP* **09** (2012) 035, doi:10.1007/JHEP09(2012)035, arXiv:1110.6926.

[7] CMS Collaboration, "Measurements of properties of the Higgs boson decaying into the four-lepton final state in pp collisions at $\sqrt{s} = 13$ TeV", *JHEP* **11** (2017) 047, doi:10.1007/JHEP11(2017)047, arXiv:1706.09936.

[8] ATLAS and CMS Collaborations, "Combined measurement of the Higgs boson mass in pp collisions at $\sqrt{s} = 7$ and 8 TeV with the ATLAS and CMS experiments", *Phys. Rev. Lett.* **114** (2015) 191803, doi:10.1103/PhysRevLett.114.191803, arXiv:1503.07589.

[9] P. Ramond, "Dual theory for free fermions", *Phys. Rev. D* **3** (1971) 2415, doi:10.1103/PhysRevD.3.2415.

[10] Y. A. Gol'fand and E. P. Likhtman, "Extension of the algebra of Poincaré group generators and violation of P invariance", *JETP Lett.* **13** (1971) 323.

[11] A. Neveu and J. H. Schwarz, "Factorizable dual model of pions", *Nucl. Phys. B* **31** (1971) 86, doi:10.1016/0550-3213(71)90448-2.

[12] D. V. Volkov and V. P. Akulov, "Possible universal neutrino interaction", *JETP Lett.* **16** (1972) 438.

[13] J. Wess and B. Zumino, "A lagrangian model invariant under supergauge transformations", *Phys. Lett. B* **49** (1974) 52, doi:10.1016/0370-2693(74)90578-4.

[14] J. Wess and B. Zumino, "Supergauge transformations in four dimensions", *Nucl. Phys. B* **70** (1974) 39, doi:10.1016/0550-3213(74)90355-1.

[15] P. Fayet, "Supergauge invariant extension of the Higgs mechanism and a model for the electron and its neutrino", *Nucl. Phys. B* **90** (1975) 104, doi:10.1016/0550-3213(75)90636-7.

[16] H. P. Nilles, "Supersymmetry, supergravity and particle physics", *Phys. Rep.* **110** (1984) 1, doi:10.1016/0370-1573(84)90008-5.

[17] G. R. Farrar and P. Fayet, "Phenomenology of the production, decay, and detection of new hadronic states associated with supersymmetry", *Phys. Lett. B* **76** (1978) 575, doi:10.1016/0370-2693(78)90858-4.

[18] P. Meade, N. Seiberg, and D. Shih, "General gauge mediation", *Prog. Theor. Phys. Suppl.* **177** (2009) 143, doi:10.1143/PTPS.177.143, arXiv:0801.3278.

[19] S. Deser and B. Zumino, "Broken supersymmetry and supergravity", *Phys. Rev. Lett.* **38** (1977) 1433, doi:10.1103/PhysRevLett.38.1433.

[20] E. Cremmer et al., "Super-higgs effect in supergravity with general scalar interactions", *Phys. Lett. B* **79** (1978) 231, doi:10.1016/0370-2693(78)90230-7.

[21] N. Arkani-Hamed et al., "MARMOSET: The path from LHC data to the new standard model via on-shell effective theories", (2007). arXiv:hep-ph/0703088.

[22] J. Alwall, P. C. Schuster, and N. Toro, "Simplified models for a first characterization of new physics at the LHC", *Phys. Rev. D* **79** (2009) 075020, doi:10.1103/PhysRevD.79.075020, arXiv:0810.3921.

[23] J. Alwall, M.-P. Le, M. Lisanti, and J. G. Wacker, "Model-independent jets plus missing energy searches", *Phys. Rev. D* **79** (2009) 015005, doi:10.1103/PhysRevD.79.015005, arXiv:0809.3264.

[24] D. Alves et al., "Simplified models for LHC new physics searches", *J. Phys. G* **39** (2012) 105005, doi:10.1088/0954-3899/39/10/105005, arXiv:1105.2838.

[25] CMS Collaboration, "Interpretation of searches for supersymmetry with simplified models", *Phys. Rev. D* **88** (2013) 052017, doi:10.1103/PhysRevD.88.052017, arXiv:1301.2175.

[26] CMS Collaboration, "Search for gauge-mediated supersymmetry in events with at least one photon and missing transverse momentum in pp collisions at $\sqrt{s} = 13$ TeV", *Phys. Lett. B* **780** (2018) 118, doi:10.1016/j.physletb.2018.02.045, arXiv:1711.08008.

[27] CMS Collaboration, "Search for supersymmetry in events with at least one photon, missing transverse momentum, and large transverse event activity in proton-proton collisions at $\sqrt{s} = 13$ TeV", *JHEP* **12** (2017) 142, doi:10.1007/JHEP12(2017)142, arXiv:1707.06193.

[28] ATLAS Collaboration, "Search for supersymmetry in a final state containing two photons and missing transverse momentum in $\sqrt{s} = 13$ TeV pp collisions at the LHC using the ATLAS detector", *Eur. Phys. J. C* **76** (2016) 517, doi:10.1140/epjc/s10052-016-4344-x, arXiv:1606.09150.

[29] ATLAS Collaboration, "Search for photonic signatures of gauge-mediated supersymmetry in 13 TeV pp collisions with the ATLAS detector", *Phys. Rev. D* **97** (2018) 092006, doi:10.1103/PhysRevD.97.092006, arXiv:1802.03158.

[30] CMS Collaboration, "The CMS experiment at the CERN LHC", *JINST* **3** (2008) S08004, doi:10.1088/1748-0221/3/08/S08004.

[31] CMS Collaboration, "The CMS trigger system", *JINST* **12** (2017) P01020, doi:10.1088/1748-0221/12/01/P01020, arXiv:1609.02366.

[32] J. Alwall et al., "The automated computation of tree-level and next-to-leading order differential cross sections, and their matching to parton shower simulations", *JHEP* **07** (2014) 079, doi:10.1007/JHEP07(2014)079, arXiv:1405.0301.

[33] M. Beneke, P. Falgari, S. Klein, and C. Schwinn, "Hadronic top-quark pair production with NNLL threshold resummation", *Nucl. Phys. B* **855** (2012) 695, doi:10.1016/j.nuclphysb.2011.10.021, arXiv:1109.1536.

[34] M. Cacciari et al., "Top-pair production at hadron colliders with next-to-next-to-leading logarithmic soft-gluon resummation", *Phys. Lett. B* **710** (2012) 612, doi:10.1016/j.physletb.2012.03.013, arXiv:1111.5869.

[35] P. Bärnreuther, M. Czakon, and A. Mitov, "Percent-level-precision physics at the Tevatron: Next-to-next-to-leading order QCD corrections to $q\bar{q} \to t\bar{t} + X$", *Phys. Rev. Lett.* **109** (2012) 132001, doi:10.1103/PhysRevLett.109.132001, arXiv:1204.5201.

[36] M. Czakon and A. Mitov, "NNLO corrections to top-pair production at hadron colliders: the all-fermionic scattering channels", *JHEP* **12** (2012) 054, doi:10.1007/JHEP12(2012)054, arXiv:1207.0236.

[37] M. Czakon and A. Mitov, "NNLO corrections to top pair production at hadron colliders: the quark-gluon reaction", *JHEP* **01** (2013) 080, doi:10.1007/JHEP01(2013)080, arXiv:1210.6832.

[38] M. Czakon, P. Fiedler, and A. Mitov, "Total top-quark pair-production cross section at hadron colliders through $O(\alpha_S^4)$", *Phys. Rev. Lett.* **110** (2013) 252004, doi:10.1103/PhysRevLett.110.252004, arXiv:1303.6254.

[39] R. Gavin, Y. Li, F. Petriello, and S. Quackenbush, "W physics at the LHC with FEWZ 2.1", *Comput. Phys. Commun.* **184** (2013) 208, doi:10.1016/j.cpc.2012.09.005, arXiv:1201.5896.

[40] R. Gavin, Y. Li, F. Petriello, and S. Quackenbush, "FEWZ 2.0: A code for hadronic z production at next-to-next-to-leading order", *Comput. Phys. Commun.* **182** (2011) 2388, doi:10.1016/j.cpc.2011.06.008, arXiv:1011.3540.

[41] R. Frederix and S. Frixione, "Merging meets matching in MC@NLO", *JHEP* **12** (2012) 061, doi:10.1007/JHEP12(2012)061, arXiv:1209.6215.

[42] A. Kalogeropoulos and J. Alwall, "The SysCalc code: A tool to derive theoretical systematic uncertainties", arXiv:1801.08401.

[43] P. Artoisenet, R. Frederix, O. Mattelaer, and R. Rietkerk, "Automatic spin-entangled decays of heavy resonances in Monte Carlo simulations", *JHEP* **03** (2013) 015, doi:10.1007/JHEP03(2013)015, arXiv:1212.3460.

[44] NNPDF Collaboration, "Parton distributions for the LHC Run II", *JHEP* **04** (2015) 040, doi:10.1007/JHEP04(2015)040, arXiv:1410.8849.

[45] T. Sjöstrand et al., "An introduction to PYTHIA 8.2", *Comput. Phys. Commun.* **191** (2015) 159, doi:10.1016/j.cpc.2015.01.024, arXiv:1410.3012.

[46] CMS Collaboration, "Event generator tunes obtained from underlying event and multiparton scattering measurements", *Eur. Phys. J.* **C76** (2016), no. 3, 155, doi:10.1140/epjc/s10052-016-3988-x, arXiv:1512.00815.

[47] J. Alwall et al., "Comparative study of various algorithms for the merging of parton showers and matrix elements in hadronic collisions", *Eur. Phys. J. C* **53** (2008) 473, doi:10.1140/epjc/s10052-007-0490-5, arXiv:0706.2569.

[48] W. Beenakker, R. Höpker, M. Spira, and P. M. Zerwas, "Squark and gluino production at hadron colliders", *Nucl. Phys. B* **492** (1997) 51, doi:10.1016/S0550-3213(97)00084-9, arXiv:hep-ph/9610490.

[49] A. Kulesza and L. Motyka, "Threshold resummation for squark-antisquark and gluino-pair production at the LHC", *Phys. Rev. Lett.* **102** (2009) 111802, doi:10.1103/PhysRevLett.102.111802, arXiv:0807.2405.

[50] A. Kulesza and L. Motyka, "Soft gluon resummation for the production of gluino-gluino and squark-antisquark pairs at the LHC", *Phys. Rev. D* **80** (2009) 095004, doi:10.1103/PhysRevD.80.095004, arXiv:0905.4749.

[51] W. Beenakker et al., "Soft-gluon resummation for squark and gluino hadroproduction", *JHEP* **12** (2009) 041, doi:10.1088/1126-6708/2009/12/041, arXiv:0909.4418.

[52] W. Beenakker et al., "Squark and gluino hadroproduction", *Int. J. Mod. Phys. A* **26** (2011) 2637, doi:10.1142/S0217751X11053560, arXiv:1105.1110.

[53] GEANT4 Collaboration, "GEANT4—a simulation toolkit", *Nucl. Instrum. Meth. A* **506** (2003) 250, doi:10.1016/S0168-9002(03)01368-8.

[54] CMS Collaboration, "The fast simulation of the CMS detector at LHC", *J. Phys. Conf. Ser.* **331** (2011) 032049, doi:10.1088/1742-6596/331/3/032049.

[55] CMS Collaboration, "Particle-flow reconstruction and global event description with the CMS detector", *JINST* **12** (2017) P10003, doi:10.1088/1748-0221/12/10/P10003, arXiv:1706.04965.

[56] CMS Collaboration, "Performance of electron reconstruction and selection with the CMS detector in proton-proton collisions at $\sqrt{s} = 8$ TeV", *JINST* **10** (2015) P06005, doi:10.1088/1748-0221/10/06/P06005, arXiv:1502.02701.

[57] CMS Collaboration, "Performance of photon reconstruction and identification with the CMS detector in proton-proton collisions at $\sqrt{s} = 8$ TeV", *JINST* **10** (2015) P08010, doi:10.1088/1748-0221/10/08/P08010, arXiv:1502.02702.

[58] CMS Collaboration, "The performance of the CMS muon detector in proton-proton collisions at $\sqrt{s} = 7$ TeV at the LHC", *JINST* **8** (2013) P11002, doi:10.1088/1748-0221/8/11/P11002, arXiv:1306.6905.

[59] M. Cacciari, G. P. Salam, and G. Soyez, "The anti-k_{T} jet clustering algorithm", *JHEP* **04** (2008) 063, doi:10.1088/1126-6708/2008/04/063, arXiv:0802.1189.

[60] M. Cacciari, G. P. Salam, and G. Soyez, "FastJet user manual", *Eur. Phys. J. C* **72** (2012) 1896, doi:10.1140/epjc/s10052-012-1896-2, arXiv:1111.6097.

[61] CMS Collaboration, "Jet performance in pp collisions at $\sqrt{s} = 7$ TeV", CMS Physics Analysis Summary CMS-PAS-JME-10-003, CERN, 2010.

[62] CMS Collaboration, "Jet energy scale and resolution in the CMS experiment in pp collisions at 8 TeV", *JINST* **12** (2017) P02014, doi:10.1088/1748-0221/12/02/P02014, arXiv:1607.03663.

[63] M. Cacciari and G. P. Salam, "Pileup subtraction using jet areas", *Phys. Lett. B* **659** (2008) 119, doi:10.1016/j.physletb.2007.09.077, arXiv:0707.1378.

[64] CMS Collaboration, "Identification of heavy-flavour jets with the CMS detector in pp collisions at 13 TeV", *JINST* **13** (2018) P05011, doi:10.1088/1748-0221/13/05/P05011, arXiv:1712.07158.

[65] K. Rehermann and B. Tweedie, "Efficient identification of boosted semileptonic top quarks at the LHC", *JHEP* **03** (2011) 059, doi:10.1007/JHEP03(2011)059, arXiv:1007.2221.

[66] CMS Collaboration, "Performance of missing energy reconstruction in 13 TeV pp collision data using the CMS detector", CMS Physics Analysis Summary CMS-PAS-JME-16-004, CERN, 2016.

[67] M. Cacciari et al., "The $t\bar{t}$ cross-section at 1.8 TeV and 1.96 TeV: a study of the systematics due to parton densities and scale dependence", *JHEP* **04** (2004) 068, doi:10.1088/1126-6708/2004/04/068, arXiv:hep-ph/0303085.

[68] S. Catani, D. de Florian, M. Grazzini, and P. Nason, "Soft gluon resummation for Higgs boson production at hadron colliders", *JHEP* **07** (2003) 028, doi:10.1088/1126-6708/2003/07/028, arXiv:hep-ph/0306211.

[69] A. Denner, S. Dittmaier, M. Hecht, and C. Pasold, "NLO QCD and electroweak corrections to $Z + \gamma$ production with leptonic Z-boson decays", *JHEP* **02** (2016) 057, doi:10.1007/JHEP02(2016)057, arXiv:1510.08742.

[70] CMS Collaboration, "Search for supersymmetry in multijet events with missing transverse momentum in proton-proton collisions at 13 TeV", *Phys. Rev. D* **96** (2017) 032003, doi:10.1103/PhysRevD.96.032003, arXiv:1704.07781.

[71] G. Cowan, K. Cranmer, E. Gross, and O. Vitells, "Asymptotic formulae for likelihood-based tests of new physics", *Eur. Phys. J. C* **71** (2011) 1554, doi:10.1140/epjc/s10052-011-1554-0, arXiv:1007.1727. [Erratum: doi:10.1140/epjc/s10052-013-2501-z].

[72] T. Junk, "Confidence level computation for combining searches with small statistics", *Nucl. Instrum. Meth. A* **434** (1999) 435, doi:10.1016/S0168-9002(99)00498-2, arXiv:hep-ex/9902006.

[73] A. L. Read, "Presentation of search results: the CL_s technique", *J. Phys. G* **28** (2002) 2693, doi:10.1088/0954-3899/28/10/313.